NeuroImage 182 (2018) 128–135

Contents lists available at ScienceDirect

NeuroImage

journal homepage: www.elsevier.com/locate/neuroimage

Modelling and interpretation of magnetization transfer imaging in the brain

John G. Sled [a,b,*]

[a] Hospital for Sick Children, Mouse Imaging Centre, Toronto, Ontario, Canada
[b] Medical Biophysics, University of Toronto, Toronto, Ontario, Canada

ARTICLE INFO

Keywords:
Magnetization transfer
Inhomogeneous magnetization transfer
Chemical exchange saturation transfer
Quantitative magnetic resonance imaging
White matter
Grey matter
Tissue microstructure

ABSTRACT

Magnetization transfer contrast has yielded insight into brain tissue microstructure changes across the lifespan and in a range of disorders. This progress has been aided by the development of quantitative magnetization transfer imaging techniques able to extract intrinsic properties of the tissue that are independent of the specifics of the data acquisition. While the tissue properties extracted by these techniques do not map directly onto specific cellular structures or pathological processes, a growing body of work from animal models and histopathological correlations aids the in vivo interpretation of magnetization transfer properties of tissue. This review examines the biophysical models that have been developed to describe magnetization transfer contrast in tissue as well as the experimental evidence for the biological interpretation of magnetization transfer data in health and disease.

Introduction

Magnetization transfer is an MRI contrast mechanism that has been used extensively to investigate tissue microstructure in the brain. First proposed for creating image contrast by Wolf and Balaban (Wolff and Balaban, 1989), this contrast mechanism is now part of the standard toolkit for research studies investigating brain development, aging, and disease (Henkelman et al., 2001). Outside of angiography applications (Pike et al., 1992), magnetization transfer contrast has been seldom used for routine clinical neuroimaging, both because the scans take longer to acquire than standard T_1- and T_2-weighted imaging and because the most easily acquired image contrast, based on magnetization transfer ratios, appears qualitatively similar to T_1-weighted scans. However for research applications, the use of magnetization transfer contrast as a quantitative measure of brain tissue structure has continued to yield new insights into changes occurring on time scales from weeks (Nossin-Manor et al., 2013) to decades (Paus et al., 2001). Magnetization transfer has had its greatest impact on the study of white matter development and disorders because of its sensitivity to myelin (Filippi and Rocca, 2004), but has also had wide application in the study of disorders affecting grey matter (Seiler et al., 2014; Tambasco et al., 2015).

The purpose of this review is to examine the biophysical models that have been proposed for magnetization transfer (MT) including recent developments in the area of inhomogeneous magnetization transfer (ihMT). These biophysical models provide the basis of so-called quantitative MT imaging methods (see for example (Sled and Pike, 2001; Ramani et al., 2002; Yarnykh, 2002)) developed to estimate intrinsic properties of the tissue that are independent of the details of the data acquisition. It should be noted that the widely used magnetization transfer ratio (MTR) is also quantitative in the sense that it yields comparable numbers in repeated measurements, however the ratios are weighted by the choice of acquisition parameters. As with other quantitative MRI methods, biophysical models of MT are expressed in terms of NMR properties such as relaxation rates, exchange rates, lineshapes, and pool sizes rather than the biochemical, cellular, and structural characteristics of brain tissue. The second part of this review examines efforts to bridge this gap by looking at the interpretations of MT in the context of the healthy and diseased brain, as well as the relationship between MT and other quantitative MRI parameters.

Tissue biophysics

Exchange and cross-relaxation

Magnetization transfer refers to the exchange of magnetization between hydrogen nuclei bound to water and hydrogen nuclei bound to semi-solid macromolecules. The latter population, while significant in number, loses transverse magnetization due to T_2 decay on a time scale of approximately 10 μs, too short for direct observation using a clinical MRI scanner. Magnetization transfer enables this hidden pool of hydrogen nuclei bound to large molecules to be detected and used to create useful tissue contrast. In thermal equilibrium there is no net transfer of

* Hospital for Sick Children, 555 University Avenue, Toronto, Ontario M5G 1X8, Canada.
E-mail address: john.sled@utoronto.ca.

https://doi.org/10.1016/j.neuroimage.2017.11.065
Received 15 May 2017; Accepted 29 November 2017
Available online 5 December 2017

magnetization between the *free* water and *restricted* macro-molecule-bound nuclei. However, manipulation of the magnetization of either the free or restricted pool of nuclei by RF pulses leads to a net magnetization transfer between the two pools that acts to restore this equilibrium. This transfer process is in addition to the usual mechanisms for nuclear magnetic relaxation by T_1 and T_2.

Magnetization transfer is thought to be mediated by through-space intermolecular dipole-dipole cross-relaxation in which the spin states of individual pairs of hydrogen nuclei are exchanged and by chemical exchange, where the nuclei themselves are exchanged. Transiently bound water molecules forming a hydration layer around the macromolecules have been proposed to facilitate dipole-dipole cross-relaxation as this process is relatively inefficient unless molecular motion is slow (Edzes and Samulski, 1977). While the residence times for water molecules in this state are typically short, less than 1 ns (Otting et al., 1991), proteins can contain pockets where water molecule residence times are longer (Otting et al., 1991; Makarov et al., 2000) and dipole-dipole cross-relaxation is efficient. Chemical exchange magnetization transfer is facilitated by the presence of hydroxyl and amine groups which can exchange rapidly with adjacent water molecules. Here the rate limiting mechanism is proposed to be the transfer of magnetization from hydrogen atoms within the macromolecule to these exchangeable groups (Liepinsh and Otting, 1996). These same mechanisms are the basis of chemical exchange saturation transfer (CEST) imaging (van Zijl and Yadav, 2011) where magnetization is exchanged between water and small mobile biomolecules.

Z-spectra

The canonical experiment for demonstrating magnetization transfer contrast is the measurement of a Z-spectrum (Grad and Bryant, 1990) (see Fig. 1). In this approach, a long period of radiofrequency excitation at a frequency offset from resonance is used to alter the magnetization state of the tissue. A short on-resonance excitation immediately following this off-resonance saturation is used to sample the longitudinal magnetization state of the water. The ratio of the detected magnetization to that measured in the absence of the off-resonance saturation yields a point on the Z-spectrum. Complete characterization of the Z-spectrum is achieved by a series of such measurements at a range of offset frequencies. While generating a Z-spectrum by this approach is not practical for clinical imaging, the Z-spectrum is useful in constructing biophysical models of MT as well as for identifying constituents of tissue that contribute to MT. In the absence of other biomolecules, the Z-spectrum follows from the Lorentzian lineshape of water. It is important to note that while this lineshape may be as narrow as a few Hz (on the order of $1/T_2$) for a well shimmed clinical scanner, the saturation process that leads to the Z-spectrum is non-linear such that, for the radiofrequency power levels used in a typical MT experiment, the long tails of the water lineshape lead to an appreciable drop in the Z-spectrum several kilohertz from resonance. This is illustrated in Fig. 1 where part of the Z-spectrum near resonance is nearly fully saturated. This *direct-effect* saturation produces a non-negligible signal in an MT experiment even in the absence of magnetization transfer and needs to be taken into account when interpreting findings from MRI studies using MT.

Magnetization transfer

The second largest and, for the present discussion, most relevant contribution to the Z-spectrum comes from the restricted-motion (macromolecular) pool of nuclei that participate in the exchange process. This includes those nuclei that exchange directly with surrounding water molecules as well as the much larger number of nuclei whose magnetization state is communicated to these exchange sites by intramolecular spin diffusion. As with the free water pool, the spectrum of frequencies where saturation of the water occurs is determined by the lineshape of the restricted motion pool, the efficiency of the exchange process, and the competing effects of magnetization recovery through T_1. Referring again to Fig. 1, the width of this spectrum is determined by $1/T_{2,r}$, where the *r* refers to the restricted-motion pool of nuclei, and for brain tissue extends approximately ±100 kHz about the resonance of water. An important step in the development of biophysical models for MT was the recognition that the lineshape of the restricted pool in biological materials is not Lorentzian (Morrison and Henkelman, 1995). The Gaussian lineshape, normally associated with NMR of solids, provides a good description of MT in materials such as agarose gel (Henkelman et al., 1993; Sled and Pike, 2000). However, for biological tissues and in particular brain tissue, the observed spectrum is better described by the super-Lorentzian lineshape (Morrison and Henkelman, 1995). This lineshape function was developed to model the situation where motion of the atomic nuclei is restricted along a particular axis such as would occur with lipid chains in a membrane (Wennerström, 1973; Bloom et al., 1986). In this model, membranes are randomly oriented, but within a given membrane, motion is restricted. A number of alternatives to the super-Lorentzian lineshape have been investigated, including empirically derived flexible lineshapes (Li et al., 1997) and a white matter specific model that takes into account the non-random orientation of membranes

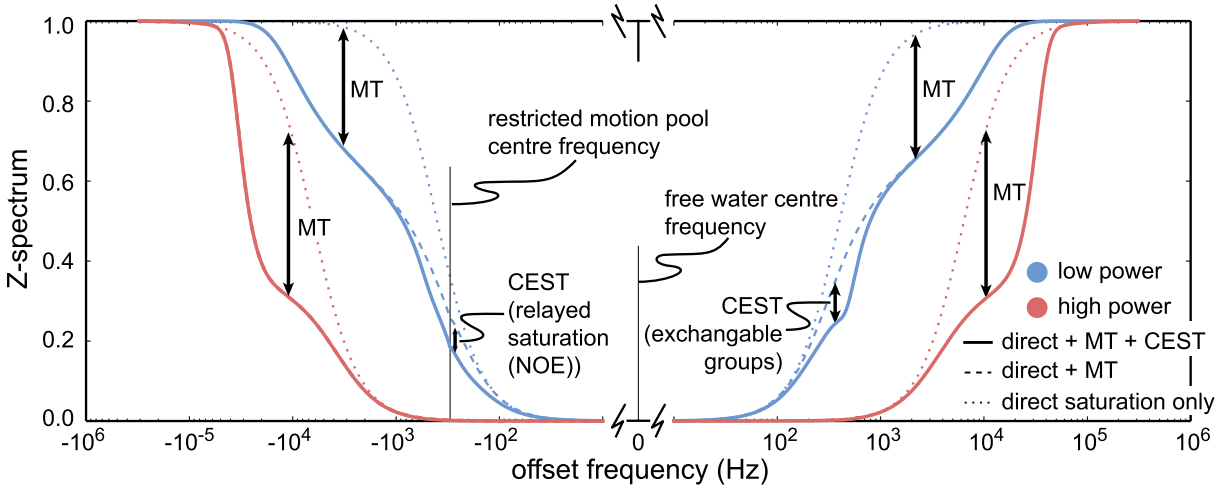

Fig. 1. Illustrative Z-spectrum showing the contributions from direct saturation of water, magnetization transfer and CEST (solid colored lines). RF excitation frequencies are reported relative to the centre frequency of water, which for this example is 300 Hz higher than the centre frequency of the restricted motion pool. The use of logarithmic negative and positive frequency axes emphasizes the near-resonance features of the curves. Also, shown are corresponding spectra where contributions from MT and/or CEST are absent (dashed and dotted colored lines). Note that, as the power of the RF excitation is increased, the near resonance part of spectrum that is nearly fully saturated widens.

in the myelin layers around an axon and the orientation of the fibres with respect to the static field (Pampel et al., 2015). Another consideration in modelling the restricted pool is that the Z-spectrum is not exactly aligned with the water resonance and has been estimated for white matter to be shifted 2.34 ppm below the resonance of water (−300 Hz at 3 T) (Hua et al., 2007). While this difference is small compared to the 100–200 kHz linewidth of the restricted motion pool this shift increases with field strength and is important for modelling the Z-spectrum near resonance and for techniques such as inhomogeneous MT, discussed subsequently, which are sensitive to asymmetry.

Chemical exchange saturation transfer

Near the water resonance a number of inflections in the Z-spectrum are observed that are associated with mobile metabolites including mobile proteins and peptides. These correspond to the lineshapes of specific chemical groups that exchange magnetization with the surrounding water. These lineshapes are narrower (longer associated T_2) due to the more rapid motion of these molecules. While the concentrations of exchangeable chemical groups are low, rapid chemical exchange with the surrounding water enables a high degree of saturation to be achieved as spins are continuously replaced during the course of irradiation. This has a non-negligible effect on the Z-spectrum and is the basis for metabolite-dependent CEST tissue contrast (Zhou et al., 2003; van Zijl and Yadav, 2011). In addition to these inflections of the Z-spectra observed at small frequency offsets above the water resonance, near-resonance inflections of the Z-spectrum are also observed below the water resonance that are proposed to arise from aliphatic and olefinic hydrogen nuclei within mobile metabolites (van Zijl et al., 2003; Jones et al., 2013). While these nuclei are not accessible to chemical exchange with water, magnetization exchange within the molecules relays the saturation of these nuclei to the surrounding water.

Inhomogeneous magnetization transfer

After accounting for a small chemical shift of the restricted-motion lineshape and the effects of mobile metabolites near resonance, the observed Z-spectrum in tissue is symmetric. This symmetry follows from the lineshape of the restricted-motion pools and the idea that, even in the presence of small variations in resonance frequency, rapid intramolecular exchange of magnetization (spin diffusion) prevents one from observing specific subpopulations of nuclei. It was therefore of considerable interest when it was recently observed in brain that Z-spectrum points measured at a fixed offset frequency, Δ, from resonance do not produce the same degree of saturated magnetization as simultaneous irradiation with an equivalent RF power at the two frequencies, −Δ and Δ, chosen symmetrically about the resonance (Varma et al., 2015a). The initial interpretation of these data was that the restricted-motion pool is not homogeneous (i.e. that RF irradiation above and below the centre frequency addresses different subpopulations of nuclei) and led to the terminology *inhomogeneous magnetization transfer* or ihMT to describe this phenomenon. Subsequent work points to a different explanation for the phenomenon but the terminology has been retained (Varma et al., 2015b; Swanson et al., 2017). Dipole-dipole interaction between nuclei such as would occur in a lipid chain is described by Provotorov theory (Goldman, 1970) in which the additional energy states created by dipole interaction are modelled as a separate and transient pool of magnetization. The differential effect of single and dual frequency excitation on this transient pool is proposed to explain ihMT. Even in the absence of dual-frequency excitation, Provotorov theory predicts measurable features in the shape of the single frequency excited Z-spectrum (Yeung et al., 1994; Morrison et al., 1995). However, this effect is small and can be neglected for RF power levels typically used in clinical MRI scans (Sled and Pike, 2001). By comparison, the ihMT experiment is a more efficient way to measure this effect and has been proposed as a more specific contrast for myelination (Varma et al., 2015a). Manning et al. (2017) developed this idea further using a model lipid system, arguing that motional averaging allowed for the system to be described in terms of the behaviour of pairs of hydrogen nuclei on methylene groups within the lipid. These pairs were modelled as a spin-1 quantum mechanical system (Slichter, 1990) and shown to reproduce the behaviour observed in ihMT experiments. Qualitatively, ihMT images of the human brain show strong grey/white matter contrast (Girard et al., 2015) with the signal arising from white matter approximately double that of grey matter (see Fig. 2).

Compartmental models of tissue

The physical processes of MT occur at atomic and molecular distances of between 0.1 and 1 nm, yet voxel sizes in MRI are typically much larger, between 500 μm and 5 mm. As a consequence magnetization transfer contrast within a given voxel may represent a mixture of cellular compartments, cell types, or even tissues. The extent to which these different compartments need to be taken into account in modelling magnetization transfer contrast continues to be an area of active investigation. As magnetization contrast in an image develops on a time scale of seconds, comparable to T_1, rapid movement of water molecules between different cellular compartments blurs these distinctions, creating the appearance of a homogeneous tissue water compartment for the purposes of MT. Contrast this with T_2 decay of water in tissue, which occurs on a time scale of 10–100 ms, enabling two or more water compartments to be resolved (MacKay et al., 1994).

Most investigations of quantitative magnetization transfer have made use of a two-pool model (Henkelman et al., 1993) representing free and restricted-motion compartments of hydrogen nuclei. A useful extension of this model is to account for the partial volume in a given voxel occupied by brain tissue and cerebrospinal fluid (Mossahebi et al., 2015). Another water compartment that has been examined with respect to MT is myelin water, the water present between the layers of myelin wrapping an axon (MacKay et al., 1994; Dortch et al., 2013b). The T_2 of this compartment is short relative to intracellular water and is proposed to rapidly exchange magnetization with macromolecules of the adjacent

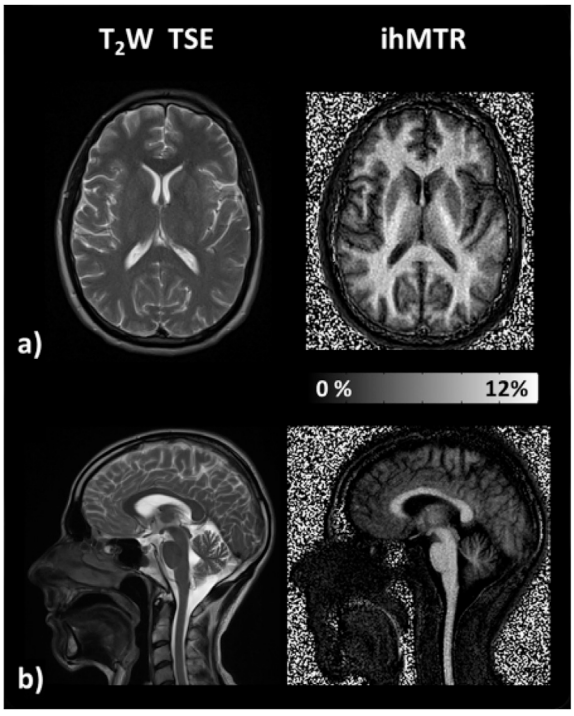

Fig. 2. Axial (a) and coronal (b) sections from an ihMT ratio contrast image. Corresponding T_2-weighted images are shown on the right. Note the strong grey/white matter contrast. Reproduced from Girard et al. (2015).

myelin (Stanisz et al., 1999). The complexity of these multicompartment models, extending the two-pool model to four pools in the case of myelin water, and the number of free parameters that must be constrained or estimated is a significant limitation to their use for imaging studies (Levesque and Pike, 2009). One means to constrain these models is to combine MT with other contrast mechanisms such as multicomponent T_2 or multicomponent diffusion measurements. One application of this approach has been for g-ratio imaging. Here diffusion based estimates of intra- and extra-cellular water fractions are combined with MT estimates of myelination to estimate the ratio of the diameter of the axon to the diameter of the myelin sheath (Stikov et al., 2015; Mohammadi et al., 2015). While dependent on a number of assumptions, models of this kind help in bridging the gap between measurable MRI parameters and cellular scale structure.

Magnetization transfer imaging

A motivation for the development of quantitative magnetization transfer imaging methods is to estimate intrinsic properties of the tissue that are independent of the details of the data acquisition. This contrasts with the more widely used MT ratio. Defined as the percent change in signal with and without MT weighting, MT ratios are affected by the RF excitation and timing parameters of the acquisition (Berry et al., 1999) as well as other tissue properties, particularly $T_{1,f}$. In practice, even for quantitative magnetization transfer imaging, acquisition details do matter in that the type of MRI acquisition technique affects the achievable resolution, potential for elevated power deposition (SAR), and coverage (e.g. 2D vs. 3D). Moreover, the choice of model and acquisition method are linked. For instance, methods that rely on off-resonance RF excitation (Sled and Pike, 2001; Ramani et al., 2002; Yarnykh, 2002) yield properties of the restricted-motion pool lineshape such as $T_{2,r}$ whereas methods using on-resonance saturation or inversion (Gochberg and Gore, 2007; Gloor et al., 2008) do not. Selecting a more complex biophysical model to describe the measured data can affect the reliability of the fitted parameters as well as the number of measurements that are required. Reducing the number of free parameters in the model, such as by using literature values for some parameters, can reduce acquisition time (Yarnykh, 2002, 2012). In addition, the precision of parameter estimates can be optimized for a given number of measurements using optimal design procedures (Cercignani and Alexander, 2006; Levesque et al., 2011).

The goal of measuring intrinsic properties of the tissue can only be realized if the MRI scanning conditions are well characterized. As the subject within the scanner affects the homogeneity of the RF field (B_1^+) and main magnetic field (B_0), it is typical to measure these fields as part of a quantitative magnetization transfer imaging protocol (Levesque et al., 2010b). Field strengths propagate non-linearly through the MT model and signal equations such that the analysis of quantitative data entails accounting for the variation in these acquisition parameters for each voxel in the image (Sled and Pike, 2001). Quantitative scan protocols tend to be longer than conventional contrast-weighted protocols, motivating the use of motion compensation when combining data for analysis. MT acquisitions making use of off-resonance RF excitation are inherently SAR intensive, a difficulty that becomes more acute for imaging humans at 7 T (Mougin et al., 2010). The total power deposition required can be reduced by making use of fast imaging protocols such as echo planar imaging or steady-state free precession techniques as well as multichannel coils and compressed sensing methods. MT imaging protocols based on off-resonance excitation use pulsed rather than continuous wave RF excitation to achieve MT contrast, which both reduces SAR and allows for optimization of the inter-pulse interval based on exchange dynamics. While a full description of the different quantitative MT imaging acquisition methods is beyond the scope of the present review, the interested reader is directed to a recent review and accompanying freely available software qMTlab (Cabana et al., 2015).

In considering the applications of quantitative MT imaging it is useful to define the most common tissue parameters that are estimated. The binary spin bath model as formulated by Henkelman et al. (1993) consists of free and restricted-motion pools of magnetization ($M_{0,f}$ and $M_{0,r}$ respectively). This is reported in units relative to a water reference or normalized such that the equilibrium magnetization of the free water pool is 1.0. Each pool has an associated T_1 and T_2. In practice, however, the T_1 of the restricted-motion pool ($T_{1,r}$) is not an observable parameter of these experiments and is fixed, typically at 1 s. The other parameters of the model are the relative size of the restricted pool (F) and the rate constants for forward and reverse exchange (k_f and k_r) between the two pools. Fig. 3 shows these parameter maps for a human adult brain. Note that the reverse exchange rate k_r, not shown in Fig. 3, is by definition k_f/F. There has been considerable variation in the symbols used to formulate the binary spin bath model. Table 1 is provided to assist in identifying equivalent notations when comparing different sources. With these definitions in mind, we can examine the biological and cellular correlates of MT contrast.

Biological correlates of magnetization transfer

One of the challenges for applying magnetization transfer imaging in the brain is that, like other MRI contrast mechanisms, a detailed understanding of the physical principles may not translate to clear predictions of the contrast that will be observed in tissue. Molecular mobility as well as the number and accessibilities of exchange sites all factor into the contribution of different classes of biomolecules to MT. In white matter, early work pointed to cholesterol (Koenig et al., 1990; Koenig, 1991) and sphingomyelin (Ceckler et al., 1992) as the dominant constituents of myelin responsible for MT. An analysis by Kucharczyk et al. (1994) examined major lipid components of white matter in a multilamellar vesicle model system at various pH levels and found that galactocerebroside had a greater effect than either cholesterol or sphingomyelin on MT. Inferences about the cellular correlates of MT contrast in the brain can be derived from the range of healthy and pathological conditions that have been examined.

Brain development and aging

Initial measurements of quantitative MT parameters from imaging healthy adult brain at 1.5T (Sled and Pike, 2001; Ramani et al., 2002; Yarnykh, 2002) made the unexpected observation that T_2 of the restricted-motion pool is nearly the same for white and grey matter (9.9–11.8 μs and 9.8–10.3 μs respectively (Sled et al., 2004)). One interpretation of this finding is that the lineshape of the restricted pool is determined by fine-scale molecular order, such as the lipid chains in membranes, that is common to different cell types and cellular organizations. In contrast, the size of the restricted-motion pool is two-fold larger in white matter than grey matter (11–14% vs. 6–7%) and shows significant variation between brain regions (Sled et al., 2004; Cercignani et al., 2005; Garcia et al., 2010; Dortch et al., 2013a).

A relevant question when applying biophysical models to tissue is the extent to which additional measurements and fitted model parameters contribute new information about tissue structure. A partial answer to this question is obtained by examining the covariance among measurements. Sled et al. (2004) examined two-pool MT model parameter covariance among white matter regions of adult brain using principal component analysis (PCA) and reported that 95% of the variance could be explained by four components. These components were: T_2 of the free water; T_2 of the restricted-motion pool ($T_{2,r}$); a component combining the pool size fraction and exchange rate; and a second component combining the T_1 of the free water and concentration of free water (proton density). While PCA is affected by the total variation in the parameters as well as the quality of the experimental design for discriminating between these parameters, this analysis demonstrated that MT provides additional information about healthy white matter structure that could not be

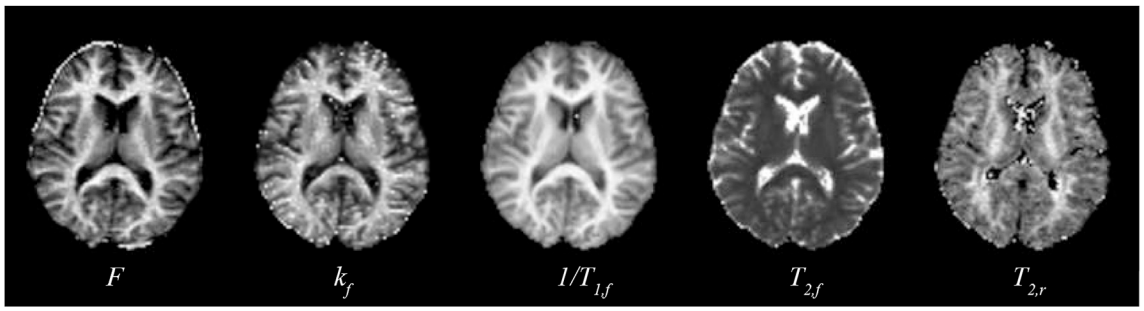

Fig. 3. Quantitative MT images of the adult human brain. The parameters shown are the pool size ratio F, the forward exchange rate k_f, the spin-lattice relaxation rate of the free pool $1/T_{1,f}$, the spin-spin relaxation rate of the free pool $T_{2,f}$, and the spin-spin relaxation rate of the restricted motion pool $T_{2,r}$. Reproduced from (Sled and Pike, 2001).

Table 1
Common symbols used to formulate the binary spin bath model for magnetization transfer.

Symbol(s)	Definition
$M_{0,f}$ or M_0^a	Equilibrium magnetization of the free pool. Some formulations define this to be 1 in arbitrary units.
$M_{0,r}$ or M_0^b	Equilibrium magnetization of the restricted pool.
F or M_0^b (where $M_0^a = 1$) or PSR	Pool size ratio. $F = M_{0,r}/M_{0,f}$.
f or BPF	Pool size fraction or bound pool fraction. $f = \frac{M_{0,r}}{M_{0,r}+M_{0,f}} = \frac{F}{1+F}$
k_f or RM_0^b or k	Forward exchange rate.
k_r or RM_0^a	Reverse exchange rate.
R or k_f/F	Exchange rate.
$T_{1,f}$ or $1/R^a$	T_1 of the free pool.
$T_{1,r}$ or $1/R^b$	T_1 of the restricted pool. Typically taken as 1 s.

obtained from measurements of T_1 and T_2 alone. A variety of examples demonstrate the additional specificity that can be gained by incorporating MT contrast. Kiefer et al. (2004) used $T_{2,r}$ estimates derived from quantitative MT imaging to discriminate hippocampal subfields. Extension of quantitative MT methods to 3D whole brain imaging by Yarnykh and Yuan (2004) demonstrated detailed white matter tract structure. Myelo-architecture of the cerebral cortex (Mangeat et al., 2015) has been visualized by combining MT ratios with $T_2^\star$ measurements. Segmentation of deep grey matter structures in the adult brain is also aided by MT contrast (Helms et al., 2009).

Early brain development is another useful context in which to examine the interpretation of magnetization transfer. The premature infant brain is largely unmyelinated and undergoes large morphological and structural changes in the weeks leading up to normal term age (Kinney et al., 1988). While quantitative MT has not been performed at this age, one can make inferences from available measurements of MT ratios and T_1 (see Fig. 4) (Nossin-Manor et al., 2012). The restricted-motion pool size is low during the preterm period, approximately 1% of free water as compared to 10–14% of free water in adult white matter. Examining the relationship between MT ratios, T_1 and water diffusion, individual structures segregate in this feature space in a way they do not were one to measure MT ratios, T_1 or diffusion alone. Comparing these data to available histological references pointed to axon density (Nossin-Manor et al., 2013) as the dominant factor driving MT during this period. While MT generally increases during early brain development, an interesting counter example is the cerebral intermediate zone (anatomically precedes formation of hemispheric white matter), suggesting that brain maturation is outpaced by brain growth in this region (Nossin-Manor et al., 2015).

MT ratios have been used to examine brain development in early childhood (1–30 months) where white matter tracts show age dependent increases in MT, with the largest changes seen in tracts projecting to primary cortical areas (Rademacher et al., 1999). Later in childhood and during adolescence, age related changes in MT are less pronounced. Interestingly, Perrin et al. (2009) when examining a large cohort (n = 404) found age related decreases in MT ratio in the white matter of

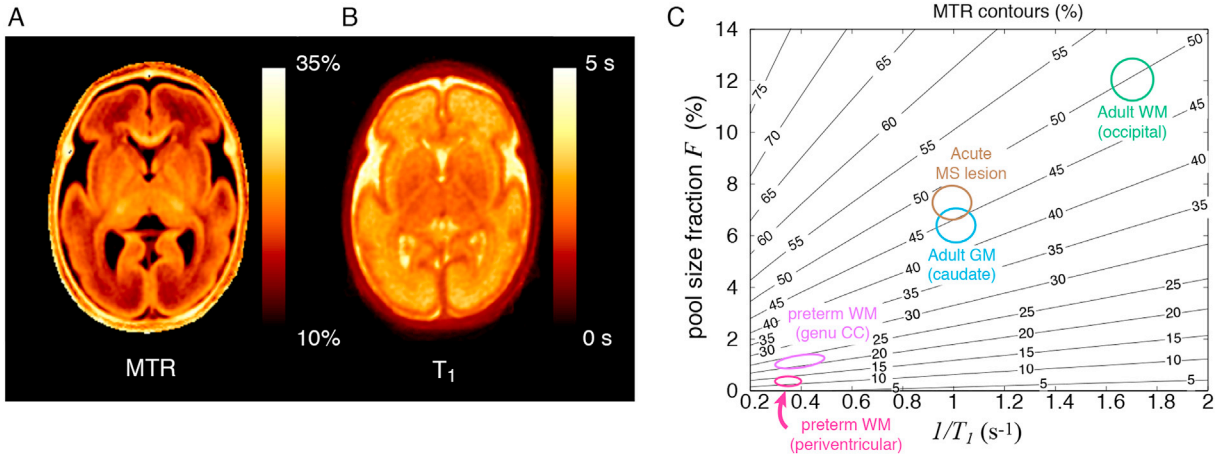

Fig. 4. A. Average MTR image for a cohort of premature infants scanned at 30.4±2 weeks gestational age. B. Average T_1 image for the same cohort. (A and B) Reproduced from (Nossin-Manor et al., 2012). C. Simulated contours of constant MT ratio (MTR) as a function of pool size fraction F and $1/T_1$. This simulation models a typical gradient echo acquisition with TR = 27 ms, flip angle = 10°, frequency offset for MT contrast of 1600 Hz and assumes values $k_f/F = 34\ s^{-1}$, $T_{2,f} = 216$ ms, and $T_{2,r} = 10\ \mu s$. F and $1/T_1$ values for preterm brain are estimated from the images at left. For comparison, literature adult and white and grey matter ranges are shown (Sled et al., 2004) along with that of acute Gd enhancing MS lesions (Levesque et al., 2010a). Note the large change in the pool size fraction between preterm and adult age as well as the affect of T_1-weighting on contours of constant MTR.

adolescent males but not adolescent females. This was proposed to be caused by testosterone-dependent axon diameter growth in males during this period. A study examining 16–55 year olds reported small age related decreases in white matter MT ratios with age (Silver et al., 1997). White matter hyperintensities, subclinical pathology with suspected vascular etiology, also become more prevalent with age and are characterized by decreased MT ratios (Maniega et al., 2015). As MT is a relatively stable MRI measure in the adult brain there has been considerable interest in its application to detect brain pathology.

White matter pathology

Magnetization transfer has been used extensively to investigate white matter disorders and in particular multiple sclerosis (MS) (Horsfield et al., 2003). White matter lesions in multiple sclerosis are characterized by a large drop in MT ratio (Brochet and Dousset, 1999; Filippi et al., 1999). Retrospective analysis of longitudinal studies have shown that these changes in MT precede lesion appearance on standard T_2-weighted scans (Filippi et al., 1998; Pike et al., 2000). Another pathological feature of MS is that normal appearing white matter is abnormal when assessed by MT (Dousset et al., 1992; Filippi et al., 1995). Measured using quantitative MT techniques, normal appearing white matter has a restricted-motion pool size (F) that is 6.5–11% smaller in patients with MS (Narayanan et al., 2006; Yarnykh et al., 2015). In comparison, acute white matter lesions in MS have a restricted-motion pool size that is on average 60% lower than healthy white matter, in addition to having reduced MT exchange rates and elevated free water T_1 and T_2 (Levesque et al., 2010a) (see Fig. 4c).

The interpretation of reduced magnetization transfer in white matter as demyelination is supported by a number of animal model and histological studies. A recent quantitative MT study examining the cuprizone mouse model (Turati et al., 2015) of pharmacologically induced demyelination and remyelination found that the size of the restricted-motion pool correlated with histological staining for myelin (Black Gold II) as well as immunofluorescent markers of myelin basic protein, a myelin constituent. In another study, micro-injection of lipopolysaccharide (LPS) was used to induce demyelinating lesions in the rat brain (Janve et al., 2013) that were examined by quantitative MT imaging. Among the in vivo quantitative MT measures, the pool size ratio (F) correlated most strongly (Pearson's correlation r = 0.89) with Luxol fast blue staining of myelin in lesions. The second highest correlation was T_1 of the free water ($T_{1,f}$) (Pearson's correlation r = 0.57). Another study using quantitative MT imaging to examine mouse optic nerve found that pool size ratio correlated with myelination but not axonal injury (Ou et al., 2009). It is important to note that while MT is sensitive to myelin content it is not specific to the process of demyelination. A pair of studies (Odrobina et al., 2005; Stanisz et al., 2004) demonstrated this in rat sciatic nerve by comparing demyelination induced by a tellurium diet to inflammation without demyelination induced by local injection of tumor necrosis factor alpha. Both models demonstrate a large decrease in MT pool size fraction; however in the inflammatory model, the distance between axons increases, effectively diluting the concentration of axons and myelin while keeping the myelin sheaths on the axons intact. In addition to these animal studies, Schmierer et al. performed quantitative MT imaging on unfixed brain slices of patients with MS (Schmierer et al., 2007). MT pool size fractions were strongly correlated to myelin staining as well as axons counted per unit area.

Grey matter pathology

Magnetization transfer has also been used to examine grey matter pathology. MT ratio differences have been reported in Alzheimer's dementia (Bozzali et al., 2001) as well as mild cognitive impairment (Kabani et al., 2002). Other applications include grey matter changes in premanifest carriers of Huntington's disease (Jurgens et al., 2010), cortical-grey-matter MT ratio changes in schizophrenia (Faget-Agius et al., 2015), and deep-grey-matter MT ratio changes in early stage Parkinson's disease (Anik et al., 2007). In addition to grey matter disorders, MT has been used to examine cortical grey matter pathology in multiple sclerosis (Derakhshan et al., 2014; Samson et al., 2014). Histopathological analysis of MS brain specimens found that MT ratio changes were associated with demyelination of cortical grey matter (Chen et al., 2013). Deep grey matter demylination detected by MT ratios has also been described in the cuprizone mouse model of demylination (Fjær et al., 2013). Quantitative MT has been less used to study grey matter, in part because of the difficulty obtaining adequate spatial resolution for cortical pathology. Kiefer et al. (2009) reported reduced $T_{2,r}$ and increased MT pool size in the anterior hippocampus of Alzheimer's disease patients and interpreted these as direct effects of amyloid-beta peptide accumulations. A recent study by Giulietti et al. (2012) found the MT exchange rate was reduced in the hippocampus as well as a number of cortical regions in Alzheimer's disease patients. While magnetization transfer between water and amyloid plaque may explain these changes, the pathophysiology of neurodegenerative disorders is complex and motivates further investigation of histopathological correlations and animal models.

Conclusions

Magnetization transfer contrast is well established among the tools for assessing tissue microstructure in the brain. While much of the work to date has made use of MT ratios, improvements in the technology for rapidly acquiring quantitative MT images of the brain has created a growing body of literature that makes use of the greater specificity afforded by these advanced techniques. MT contrast is useful for brain imaging across the whole lifespan and has applications in a range of disorders affecting grey matter and white matter. The recent introduction of ihMT contrast has the potential to expand these applications by improving the specificity of the technique. It is important to recognize however that MT, like most MRI contrast mechanisms, is determined by processes on a molecular and atomic scale and, as a consequence, is not specific to any single cellular mechanism. Interpretation of these data therefore needs to take into account the pathophysiology of the disease, supporting data from model systems and histopathology, as well as measurements using other imaging modalities. Approaching 30 years since its introduction, much work yet remains to fulfill the potential of this technology.

Acknowledgments

I would like to thank Sharon Portnoy and Lindsay Cahill for their helpful discussions in preparing this manuscript.

References

Anik, Y., Iseri, P., Demirci, A., Komsuoglu, S., Inan, N., 2007. Magnetization transfer ratio in early period of Parkinson disease. Acad. Radiol. 14 (2), 189–192.

Berry, I., Barker, G., Barkhof, F., Campi, A., Dousset, V., Franconi, J., Gass, A., Schreiber, W., Miller, D., Tofts, P., 1999. A multicenter measurement of magnetization transfer ratio in normal white matter. J. Magn. Reson Imaging 9 (3), 441–446.

Bloom, M., Holmes, K.T., Mountford, C.E., Williams, P.G., 1986. Complete proton magnetic resonance in whole cells. J. Magnetic Reson. 69, 73–91.

Bozzali, M., Franceschi, M., Falini, A., Pontesilli, S., Cercignani, M., Magnani, G., Scotti, G., Comi, G., Filippi, M., 2001. Quantification of tissue damage in AD using diffusion tensor and magnetization transfer MRI. Neurology 57 (6), 1135–1137.

Brochet, B., Dousset, V., 1999. Pathological correlates of magnetization transfer imaging abnormalities in animal models and humans with multiple sclerosis. Neurology 53 (5 Suppl. 3), S12–S17, 17 refs, Review.

Cabana, J.-F., Gu, Y., Boudreau, M., Levesque, I.R., Atchia, Y., Sled, J.G., Narayanan, S., Arnold, D.L., Pike, G.B., Cohen-Adad, J., Duval, T., Vuong, M.-T., Stikov, N., 2015. Quantitative magnetization transfer imaging *made* easy with *q*MT*Lab* : software for data simulation, analysis, and visualization. Concepts Magn. Reson 44A (5), 263–277.

Ceckler, T.L., Wolff, S.D., Simon, A., Yip, V., Balaban, R.S., 1992. Dynamic and chemical factors affecting water proton relaxation by macromolecules. J. Magnetic Reson. 98, 637–645.

Cercignani, M., Alexander, D., 2006. Optimal acquisition schemes for in vivo quantitative magnetization transfer MRI. Magn. Reson Med. 56 (4), 803–810.
Cercignani, M., Symms, M., Schmierer, K., Boulby, P., Tozer, D., Ron, M., Tofts, P., Barker, G., 2005. Three-dimensional quantitative magnetisation transfer imaging of the human brain. NeuroImage 27 (2), 436–441.
Chen, J., Easley, K., Schneider, C., Nakamura, K., Kidd, G., Chang, A., Staugaitis, S., Fox, R., Fisher, E., Arnold, D., Trapp, B., 2013. Clinically feasible MTR is sensitive to cortical demyelination in MS. Neurology 80 (3), 246–252.
Derakhshan, M., Caramanos, Z., Narayanan, S., Arnold, D., Louis Collins, D., 2014. Surface-based analysis reveals regions of reduced cortical magnetization transfer ratio in patients with multiple sclerosis: a proposed method for imaging subpial demyelination. Hum. Brain Mapp. 35 (7), 3402–3413.
Dortch, R., Moore, J., Li, K., Jankiewicz, M., Gochberg, D., Hirtle, J., Gore, J., Smith, S., 2013a. Quantitative magnetization transfer imaging of human brain at 7 T. NeuroImage 64, 640–649.
Dortch, R.D., Harkins, K.D., Juttukonda, M.R., Gore, J.C., Does, M.D., 2013b. Characterizing inter-compartmental water exchange in myelinated tissue using relaxation exchange spectroscopy: REXSY in optic and sciatic nerve. Magn. Reson. Med. 70 (5), 1450–1459.
Dousset, V., Grossman, R.I., Ramer, K.N., Schnall, M.D., Young, L.H., Gonzalez-Scarano, F., Lavi, E., Cohen, J.A., Feb 1992. Experimental allergic encephalomyelitis and multiple sclerosis: lesion characterization with magnetization transfer imaging [published erratum appears in Radiology 1992 Jun;183(3):878]. Radiology 182 (2), 483–491.
Edzes, H.T., Samulski, E.D., 1977. Cross relaxation and spin diffusion in the proton NMR of hydrated collagen. Nature 265, 521–523.
Faget-Agius, C., Catherine, F., Boyer, L., Wirsich, J., Jonathan, W., Ranjeva, J., Jean-Philippe, R., Richieri, R., Raphaelle, R., Soulier, E., Elisabeth, S., Confort-Gouny, S., Sylviane, C., Auquier, P., Pascal, A., Guye, M., Maxime, G., Lançon, C., Christophe, L., 2015. Neural substrate of quality of life in patients with schizophrenia: a magnetisation transfer imaging study. Sci. Rep. 5, 17650.
Filippi, M., Campi, A., Dousset, V., Baratti, C., Martinelli, V., Canal, N., Scotti, G., Comi, G., Mar 1995. A magnetization transfer imaging study of normal-appearing white matter in multiple sclerosis. Neurology 45 (3 Pt 1), 478–482.
Filippi, M., Rocca, M., 2004. Magnetization transfer magnetic resonance imaging in the assessment of neurological diseases. J. Neuroimaging 14 (4), 303–313.
Filippi, M., Rocca, M., Martino, G., Horsfield, M., Comi, G., 1998. Magnetization transfer changes in the normal appearing white matter precede the appearance of enhancing lesions in patients with multiple sclerosis. Ann. Neurol. 43 (6), 809–814.
Filippi, M., Rocca, M.A., Minicucci, L., Martinelli, V., Ghezzi, A., Bergamaschi, R., Comi, G., Mar 10 1999. Magnetization transfer imaging of patients with definite ms and negative conventional MRI. Neurology 52 (4), 845–848.
Fjær, S., Bø, L., Lundervold, A., Myhr, K., Pavlin, T., Torkildsen, O., Wergeland, S., 2013. Deep gray matter demyelination detected by magnetization transfer ratio in the cuprizone model. PLoS One 8 (12), e84162.
Garcia, M., Gloor, M., Wetzel, S., Radue, E., Scheffler, K., Bieri, O., 2010. Characterization of normal appearing brain structures using high-resolution quantitative magnetization transfer steady-state free precession imaging. NeuroImage 52 (2), 532–537.
Girard, O., Prevost, V., Varma, G., Cozzone, P., Alsop, D., Duhamel, G., 2015. Magnetization transfer from inhomogeneously broadened lines (ihMT): experimental optimization of saturation parameters for human brain imaging at 1.5 tesla. Magn. Reson Med. 73 (6), 2111–2121.
Giulietti, G., Bozzali, M., Figura, V., Spanò, B., Perri, R., Marra, C., Lacidogna, G., Giubilei, F., Caltagirone, C., Cercignani, M., 2012. Quantitative magnetization transfer provides information complementary to grey matter atrophy in alzheimer's disease brains. NeuroImage 59 (2), 1114–1122.
Gloor, M., Scheffler, K., Bieri, O., 2008. Quantitative magnetization transfer imaging using balanced SSFP. Magn. Reson Med. 60 (3), 691–700.
Gochberg, D., Gore, J., 2007. Quantitative magnetization transfer imaging via selective inversion recovery with short repetition times. Magn. Reson Med. 57 (2), 437–441.
Goldman, M., 1970. Spin Temperature and Nuclear Magnetic Resoance in Solids. Oxford University Press, London.
Grad, J., Bryant, R.G., 1990. Nuclear magnetic cross-relaxation spectroscopy. J. Magnetic Reson. 90, 1–8.
Helms, G., Draganski, B., Frackowiak, R., Ashburner, J., Weiskopf, N., 2009. Improved segmentation of deep brain grey matter structures using magnetization transfer (MT) parameter maps. NeuroImage 47 (1), 194–198.
Henkelman, R., Huang, X., Xiang, Q., Stanisz, G., Swanson, S., Bronskill, M., 1993. Quantitative interpretation of magnetization transfer. Magn. Reson Med. 29 (6), 759–766.
Henkelman, R., Stanisz, G., Graham, S., 2001. Magnetization transfer in MRI: a review. NMR Biomed. 14 (2), 57–64.
Horsfield, M., Barker, G., Barkhof, F., Miller, D., Thompson, A., Filippi, M., 2003. Guidelines for using quantitative magnetization transfer magnetic resonance imaging for monitoring treatment of multiple sclerosis. J. Magn. Reson Imaging 17 (4), 389–397.
Hua, J., Jones, C., Blakeley, J., Smith, S., van Zijl, P., Zhou, J., 2007. Quantitative description of the asymmetry in magnetization transfer effects around the water resonance in the human brain. Magn. Reson Med. 58 (4), 786–793.
Janve, V., Zu, Z., Yao, S., Li, K., Zhang, F., Wilson, K., Ou, X., Does, M., Subramaniam, S., Gochberg, D., 2013. The radial diffusivity and magnetization transfer pool size ratio are sensitive markers for demyelination in a rat model of type III multiple sclerosis (MS) lesions. NeuroImage 74, 298–305.
Jones, C., Huang, A., Xu, J., Edden, R., Schär, M., Hua, J., Oskolkov, N., Zacà, D., Zhou, J., McMahon, M., Pillai, J., van Zijl, P., 2013. Nuclear overhauser enhancement (NOE) imaging in the human brain at 7T. NeuroImage 77, 114–124.
Jurgens, C., Bos, R., Luyendijk, J., Witjes-Ané, M., van der Grond, J., Middelkoop, H., Roos, R., 2010. Magnetization transfer imaging in 'premanifest' huntington's disease. J. Neurol. 257 (3), 426–432.
Kabani, N., Sled, J., Chertkow, H., 2002. Magnetization transfer ratio in mild cognitive impairment and dementia of alzheimer's type. NeuroImage 15 (3), 604–610.
Kiefer, C., Brockhaus, L., Cattapan-Ludewig, K., Ballinari, P., Burren, Y., Schroth, G., Wiest, R., 2009. Multi-parametric classification of alzheimer's disease and mild cognitive impairment: the impact of quantitative magnetization transfer MR imaging. NeuroImage 48 (4), 657–667.
Kiefer, C., Slotboom, J., Buri, C., Gralla, J., Remonda, L., Dierks, T., Strik, W., Schroth, G., Kalus, P., 2004. Differentiating hippocampal subregions by means of quantitative magnetization transfer and relaxometry: preliminary results. NeuroImage 23 (3), 1093–1099.
Kinney, H., Brody, B., Kloman, A., Gilles, F., 1988. Sequence of central nervous system myelination in human infancy. II. patterns of myelination in autopsied infants. J. Neuropathol. Exp. Neurol. 47 (3), 217–234.
Koenig, S.H., 1991. Cholesterol of myelin is the determinant of gray-white contrast in MRI of brain. Magnetic Reson. Med. 20 (2), 285–291.
Koenig, S.H., Brown, R.D., Spiller, M., Lundbom, N., 1990. Relaxometry of brain: why white matter appears bright in MRI. Magn. Reson. Med. 14 (3), 482–495.
Kucharczyk, W., Macdonald, P., Stanisz, G., Henkelman, R., 1994. Relaxivity and magnetization transfer of white matter lipids at MR imaging: importance of cerebrosides and pH. Radiology 192 (2), 521–529.
Levesque, I., Giacomini, P., Narayanan, S., Ribeiro, L., Sled, J., Arnold, D., Pike, G., 2010a. Quantitative magnetization transfer and myelin water imaging of the evolution of acute multiple sclerosis lesions. Magn. Reson Med. 63 (3), 633–640.
Levesque, I., Pike, G., 2009. Characterizing healthy and diseased white matter using quantitative magnetization transfer and multicomponent T(2) relaxometry: a unified view via a four-pool model. Magn. Reson Med. 62 (6), 1487–1496.
Levesque, I., Sled, J., Narayanan, S., Giacomini, P., Ribeiro, L., Arnold, D., Pike, G., 2010b. Reproducibility of quantitative magnetization-transfer imaging parameters from repeated measurements. Magn. Reson Med. 64 (2), 391–400.
Levesque, I., Sled, J., Pike, G., 2011. Iterative optimization method for design of quantitative magnetization transfer imaging experiments. Magn. Reson Med. 66 (3), 635–643.
Li, J., Graham, S., Henkelman, R., 1997. A flexible magnetization transfer line shape derived from tissue experimental data. Magn. Reson Med. 37 (6), 866–871.
Liepinsh, E., Otting, G., 1996. Proton exchange rates from amino acid side chains–implications for image contrast. Magn. Reson Med. 35 (1), 30–42.
MacKay, A., Whittall, K., Adler, J., Li, D., Paty, D., Graeb, D., 1994. In vivo visualization of myelin water in brain by magnetic resonance. Magn. Reson Med. 31 (6), 673–677.
Makarov, V., Andrews, B., Smith, P., Pettitt, B., 2000. Residence times of water molecules in the hydration sites of myoglobin. Biophys. J. 79 (6), 2966–2974.
Mangeat, G., Govindarajan, S., Mainero, C., Cohen-Adad, J., 2015. Multivariate combination of magnetization transfer, T2* and B0 orientation to study the myelo-architecture of the in vivo human cortex. NeuroImage 119, 89–102.
Maniega, S., Valdés Hernández, M., Clayden, J., Royle, N., Murray, C., Morris, Z., Aribisala, B., Gow, A., Starr, J., Bastin, M., Deary, I., Wardlaw, J., 2015. White matter hyperintensities and normal-appearing white matter integrity in the aging brain. Neurobiol. Aging 36 (2), 909–918.
Manning, A., Chang, K., MacKay, A., Michal, C., 2017. The physical mechanism of "inhomogeneous" magnetization transfer MRI. J. Magn. Reson 274, 125–136.
Mohammadi, S., Carey, D., Dick, F., Diedrichsen, J., Sereno, M., Reisert, M., Callaghan, M., Weiskopf, N., 2015. Whole-brain in-vivo measurements of the axonal g-ratio in a group of 37 healthy volunteers. Front. Neurosci. 9, 441.
Morrison, C., Henkelman, R., 1995. A model for magnetization transfer in tissues. Magn. Reson Med. 33 (4), 475–482.
Morrison, C., Stanisz, G., Henkelman, R., 1995. Modeling magnetization transfer for biological-like systems using a semi-solid pool with a super-lorentzian lineshape and dipolar reservoir. J. Magn. Reson B 108 (2), 103–113.
Mossahebi, P., Alexander, A., Field, A., Samsonov, A., 2015. Removal of cerebrospinal fluid partial volume effects in quantitative magnetization transfer imaging using a three-pool model with nonexchanging water component. Magn. Reson Med. 74 (5), 1317–1326.
Mougin, O., Coxon, R., Pitiot, A., Gowland, P., 2010. Magnetization transfer phenomenon in the human brain at 7 t. NeuroImage 49 (1), 272–281.
Narayanan, S., Francis, S., Sled, J., Santos, A., Antel, S., Levesque, I., Brass, S., Lapierre, Y., Sappey-Marinier, D., Pike, G., Arnold, D., 2006. Axonal injury in the cerebral normal-appearing white matter of patients with multiple sclerosis is related to concurrent demyelination in lesions but not to concurrent demyelination in normal-appearing white matter. NeuroImage 29 (2), 637–642.
Nossin-Manor, R., Card, D., Morris, D., Noormohamed, S., Shroff, M., Whyte, H., Taylor, M., Sled, J., 2013. Quantitative MRI in the very preterm brain: assessing tissue organization and myelination using magnetization transfer, diffusion tensor and T1 imaging. NeuroImage 64, 505–516.
Nossin-Manor, R., Card, D., Raybaud, C., Taylor, M., Sled, J., 2015. Cerebral maturation in the early preterm period-a magnetization transfer and diffusion tensor imaging study using voxel-based analysis. NeuroImage 112, 30–42.
Nossin-Manor, R., Chung, A., Whyte, H., Shroff, M., Taylor, M., Sled, J., 2012. Deep gray matter maturation in very preterm neonates: regional variations and pathology-related age-dependent changes in magnetization transfer ratio. Radiology 263 (2), 510–517.

Odrobina, E., Lam, T., Pun, T., Midha, R., Stanisz, G., 2005. MR properties of excised neural tissue following experimentally induced demyelination. NMR Biomed. 18 (5), 277–284.
Otting, G., Liepinsh, E., Wthrich, K., 1991. Protein hydration in aqueous solution. Science 254 (5034), 974–980.
Ou, X., Sun, S., Liang, H., Song, S., Gochberg, D., 2009. Quantitative magnetization transfer measured pool-size ratio reflects optic nerve myelin content in ex vivo mice. Magn. Reson Med. 61 (2), 364–371.
Pampel, A., Müller, D., Anwander, A., Marschner, H., Möller, H., 2015. Orientation dependence of magnetization transfer parameters in human white matter. NeuroImage 114, 136–146.
Paus, T., Collins, D., Evans, A., Leonard, G., Pike, B., Zijdenbos, A., 2001. Maturation of white matter in the human brain: a review of magnetic resonance studies. Brain Res. Bull. 54 (3), 255–266.
Perrin, J., Leonard, G., Perron, M., Pike, G., Pitiot, A., Richer, L., Veillette, S., Pausova, Z., Paus, T., 2009. Sex differences in the growth of white matter during adolescence. NeuroImage 45 (4), 1055–1066.
Pike, G., De Stefano, N., Narayanan, S., Worsley, K., Pelletier, D., Francis, G., Antel, J., Arnold, D., 2000. Multiple sclerosis: magnetization transfer MR imaging of white matter before lesion appearance on t2-weighted images. Radiology 215 (3), 824–830.
Pike, G., Hu, B., Glover, G., Enzmann, D., 1992. Magnetization transfer time-of-flight magnetic resonance angiography. Magn. Reson Med. 25 (2), 372–379.
Rademacher, J., Engelbrecht, V., Bürgel, U., Freund, H., Zilles, K., 1999. Measuring in vivo myelination of human white matter fiber tracts with magnetization transfer MR. NeuroImage 9 (4), 393–406.
Ramani, A., Dalton, C., Miller, D., Tofts, P., Barker, G., 2002. Precise estimate of fundamental in-vivo MT parameters in human brain in clinically feasible times. Magn. Reson. Imaging 20 (10), 721–731.
Samson, R., Cardoso, M., Muhlert, N., Sethi, V., Wheeler-Kingshott, C., Ron, M., Ourselin, S., Miller, D., Chard, D., 2014. Investigation of outer cortical magnetisation transfer ratio abnormalities in multiple sclerosis clinical subgroups. Mult. Scler. 20 (10), 1322–1330.
Schmierer, K., Tozer, D., Scaravilli, F., Altmann, D., Barker, G., Tofts, P., Miller, D., 2007. Quantitative magnetization transfer imaging in postmortem multiple sclerosis brain. J. Magn. Reson Imaging 26 (1), 41–51.
Seiler, S., Ropele, S., Schmidt, R., 2014. Magnetization transfer imaging for in vivo detection of microstructural tissue changes in aging and dementia: a short literature review. J. Alzheimers Dis. 42 (Suppl. 3), S229–S237.
Silver, N., Barker, G., MacManus, D., Tofts, P., Miller, D., 1997. Magnetisation transfer ratio of normal brain white matter: a normative database spanning four decades of life. J. Neurol. Neurosurg. Psychiatry 62 (3), 223–228.
Sled, J., Levesque, I., Santos, A., Francis, S., Narayanan, S., Brass, S., Arnold, D., Pike, G., 2004. Regional variations in normal brain shown by quantitative magnetization transfer imaging. Magn. Reson Med. 51 (2), 299–303.
Sled, J., Pike, G., 2000. Quantitative interpretation of magnetization transfer in spoiled gradient echo MRI sequences. J. Magn. Reson 145 (1), 24–36.
Sled, J., Pike, G., 2001. Quantitative imaging of magnetization transfer exchange and relaxation properties in vivo using MRI. Magnetic Reson. Med. 46 (5), 923–931.
Slichter, C., 1990. Principles of Magnetic Resonance. Springer, Verlag.
Stanisz, G., Kecojevic, A., Bronskill, M., Henkelman, R., 1999. Characterizing white matter with magnetization transfer and T(2). Magn. Reson Med. 42 (6), 1128–1136.
Stanisz, G., Webb, S., Munro, C., Pun, T., Midha, R., 2004. MR properties of excised neural tissue following experimentally induced inflammation. Magn. Reson Med. 51 (3), 473–479.
Stikov, N., Campbell, J., Stroh, T., Lavelée, M., Frey, S., Novek, J., Nuara, S., Ho, M., Bedell, B., Dougherty, R., Leppert, I., Boudreau, M., Narayanan, S., Duval, T., Cohen-Adad, J., Picard, P., Gasecka, A., Côté, D., Pike, G., 2015. In vivo histology of the myelin g-ratio with magnetic resonance imaging. NeuroImage 118, 397–405.
Swanson, S., Malyarenko, D., Fabiilli, M., Welsh, R., Nielsen, J., Srinivasan, A., 2017. Molecular, dynamic, and structural origin of inhomogeneous magnetization transfer in lipid membranes. Magn. Reson Med. 77 (3), 1318–1328.
Tambasco, N., Nigro, P., Romoli, M., Simoni, S., Parnetti, L., Calabresi, P., 2015. Magnetization transfer MRI in dementia disorders, Huntington's disease and parkinsonism. J. Neurol. Sci. 353 (1–2), 1–8.
Turati, L., Moscatelli, M., Mastropietro, A., Dowell, N., Zucca, I., Erbetta, A., Cordiglieri, C., Brenna, G., Bianchi, B., Mantegazza, R., Cercignani, M., Baggi, F., Minati, L., 2015. In vivo quantitative magnetization transfer imaging correlates with histology during de- and remyelination in cuprizone-treated mice. NMR Biomed. 28 (3), 327–337.
van Zijl, P., Yadav, N., 2011. Chemical exchange saturation transfer (CEST): what is in a name and what isn't. Magn. Reson Med. 65 (4), 927–948.
van Zijl, P., Zhou, J., Mori, N., Payen, J., Wilson, D., Mori, S., 2003. Mechanism of magnetization transfer during on-resonance water saturation. a new approach to detect mobile proteins, peptides, and lipids. Magn. Reson Med. 49 (3), 440–449.
Varma, G., Duhamel, G., de Bazelaire, C., Alsop, D., 2015a. Magnetization transfer from inhomogeneously broadened lines: a potential marker for myelin. Magn. Reson Med. 73 (2), 614–622.
Varma, G., Girard, O., Prevost, V., Grant, A., Duhamel, G., Alsop, D., 2015b. Interpretation of magnetization transfer from inhomogeneously broadened lines (ihMT) in tissues as a dipolar order effect within motion restricted molecules. J. Magn. Reson 260, 67–76.
Wennerström, H., 1973. Proton nuclear magnetic resonance lineshapes in lamellar liquid crystals. Chem. Phys. Lett. 18 (1), 41–44.
Wolff, S., Balaban, R., 1989. Magnetization transfer contrast (MTC) and tissue water proton relaxation in vivo. Magn. Reson Med. 10 (1), 135–144.
Yarnykh, V., 2002. Pulsed z-spectroscopic imaging of cross-relaxation parameters in tissues for human MRI: theory and clinical applications. Magn. Reson Med. 47 (5), 929–939.
Yarnykh, V., 2012. Fast macromolecular proton fraction mapping from a single off-resonance magnetization transfer measurement. Magn. Reson Med. 68 (1), 166–178.
Yarnykh, V., Bowen, J., Samsonov, A., Repovic, P., Mayadev, A., Qian, P., Gangadharan, B., Keogh, B., Maravilla, K., Jung Henson, L., 2015. Fast whole-brain three-dimensional macromolecular proton fraction mapping in multiple sclerosis. Radiology 274 (1), 210–220.
Yarnykh, V., Yuan, C., 2004. Cross-relaxation imaging reveals detailed anatomy of white matter fiber tracts in the human brain. NeuroImage 23 (1), 409–424.
Yeung, H.N., Adler, R.S., Swanson, S.D., 1994. Transient decay of longitudinal magnetization in hetrogeneous spin systems under selective saturation. IV. Reformulation of the spin-bath-model equations by the Redfield-Provotorov theory. J. Magnetic Reson. A 106, 37–45.
Zhou, J., Lal, B., Wilson, D., Laterra, J., van Zijl, P., 2003. Amide proton transfer (APT) contrast for imaging of brain tumors. Magn. Reson Med. 50 (6), 1120–1126.